Buoyancy-driven instability of an autocatalytic reaction front in a Hele-Shaw cell

J. Martin,* N. Rakotomalala, D. Salin, and M. Böckmann
Laboratoire Fluides Automatique et Systèmes Thermiques, Universités Pierre et Marie Curie and Paris Sud, CNRS UMR No. 7608, Campus Universitaire, Bâtiment 502, 91405 Orsay Cedex, France
(Received 30 November 2001; published 20 May 2002)

An autocatalytic reaction-diffusion front between two reacting species may propagate as a solitary wave, namely, at constant velocity and with a stationary concentration profile. Recent experiments on such reactions have been reported to be buoyancy unstable, under certain conditions. We calculate the linear dispersion relation of the resulting instability, by applying our recent analysis of the Rayleigh-Taylor instability of two miscible fluids in a Hele-Shaw cell. The computed dispersion relation as well as our three-dimensional lattice Bhatnagar-Gross-Krook (BGK) simulations fit reasonably well experimental growth rates reported previously.

DOI: 10.1103/PhysRevE.65.051605 PACS number(s): 47.20.Bp, 47.54.+r, 47.55.Mh, 47.70.Fw

I. INTRODUCTION

Chemical reactions with autocatalytic kinetics show fascinating phenomena such as temporal oscillations and chaos, spatial stationary Turing patterns, or propagation of single fronts or wave trains [1]. Among other reactions, the oxidation of arsenous acid by iodate, the so-called IAA reaction, has been studied as a paradigm for the simple, monostable case. In this reaction, a planar front develops between the reacted and unreacted regions, and propagates as a solitary wave with a constant front velocity and a stationary concentration profile [2]. This is a result of the balance between diffusion and chemical reaction. As the reaction product is slightly lighter than the initial reactant solution [3–5], ascending reaction fronts may be buoyancy unstable, leading to a Rayleigh-Taylor (RT) instability [6–8]. This instability has been investigated experimentally in tubes [3] and in Hele-Shaw (HS) cells [4,5] (which consist of two parallel plates separated by a gap of a small thickness h).

The configuration corresponds to an unstable density profile between two miscible fluids (i.e., without any surface tension), of a finite extent. It has been recently studied for the HS geometry in the absence of a reaction [9,10]. It was first found that the transversely averaged flow in the plane of the cell can be described by a two-dimensional Navier-Stokes-Darcy equation (the NSD equation, which is similar to Brinkman's equation), which reduces to Darcy's law at small gap thickness. It was also shown that, for a given density difference, the strength of the instability is mitigated by molecular diffusion processes, by the viscous friction in the gap of the cell, and by the spatial extension of the density profile. The last two stabilizing processes enter into play when the gap width h is smaller and the extension of the front l_r larger, respectively, than the characteristic miscible Rayleigh-Taylor (MRT) length L defined below (and which involves the density contrast and the viscous and molecular diffusion coefficients [9]).

In the presence of an IAA reaction, however, the situation is different, due to the coupling between hydrodynamic instability and chemical reaction. During the last decade, several two-dimensional linear analyses have been proposed to model this instability of the ascending IAA reaction front in a HS geometry. The majority are based on the eikonal equation [11–15]. However, this does not take into account the extension of the density profile and has been shown to be questionable [16]. A few analyses use the full convection-diffusion-reaction (CDR) equation for the chemical wave and Darcy's law for the hydrodynamics [16,17] (to be denoted below as the Darcy-CDR model). Comparison of these analyses with recent measurements [5] is not fully satisfactory, however. This is particularly the case for the larger thickness HS cells (e.g., $h=900\ \mu$m), which might be attributed to the failure of Darcy's law under such conditions. The NSD equation has also been used together with the eikonal equation [12,14] (the NSD-eikonal model), but with limited success.

The objective of the present work is to apply a more comprehensive approach, based on our recent analysis of the RT instability of miscible fluids in a Hele-Shaw cell [9], by combining the convection-diffusion-reaction of the chemical process and the NSD equation (the NSD-CDR model). In general, the problem involves three characteristic length scales: the thickness of the cell h, the MRT length L, and the chemical front width l_r. The latter two are defined respectively as follows:

$$L=\left(\frac{2\rho_0\nu D}{\Delta\rho g}\right)^{1/3} \quad \text{and} \quad l_r=\sqrt{\frac{2D}{\alpha}} \tag{1}$$

where the various symbols are introduced below. The validity of the different models, which depends on the relative values of these lengths, will be addressed below. In addition, we will compare the various dispersion relations with three-dimensional (3D) lattice Bhatnagar-Gross-Krook (BGK) simulations to be conducted for this geometry [18,19], as well as with reported experimental data [5].

II. CHEMICAL WAVES

For arsenous acid in stochiometric excess and a low pH value [20], the IAA reaction is autocatalytic in iodide, and its kinetics can be modeled by the cubic rate law $f=\alpha C(C+C_S)(1-C)$, where α and $C_S>0$ include the reaction rate

*Electronic address: martin@fast.p-sud.fr

constants, and C is the concentration of iodide, normalized by the initial concentration of iodate. In the absence of bulk flow, the evolution of a solution initially free of iodide ($C=0$) toward the final reacted state ($C=1$) obeys the diffusion-reaction equation

$$\frac{\partial C}{\partial t} = D\triangle C + f(C) \tag{2}$$

where D is the molecular diffusion coefficient of iodide. When the reaction is initiated in a horizontal plane of a vertical HS cell (either by introducing some reactant or thanks to an electrode [5]), there exists a 1D traveling wave solution of Eq. (2) traveling at constant velocity along the $z^\star$ axis (from the $C=1$ to $C=0$ regions) and given by

$$C(z^\star,t) = \frac{1}{1+\exp(z^\star - v_r t)/l_r} \tag{3}$$

where the velocity v_r is

$$v_r = \sqrt{\frac{\alpha D}{2}}(1+2C_S) = \frac{D}{l_r}(1+2C_S). \tag{4}$$

This is a solitary wave, with the stationary profile resulting from a balance between diffusion and reaction [2–5,12]. As the reaction produces a lighter reacted solution, however, an upward propagating front [Eq. (3) with an upwards $z^\star$ axis] is buoyancy unstable. The concentration profile will generate an RT instability, inducing nonhomogeneous fluid velocities which will interfere with the evolution of C due to advection. In the following, we will study the stability of this ascending wave front and discuss the interplay between the chemical reaction and the instability-induced fluid velocity field.

III. LINEAR STABILITY ANALYSIS OF THE FRONT

The above-derived 1D base state consists of a mixture of two miscible fluids of a concentration profile $C(z^\star,t)$ varying along the upward vertical coordinate $z^\star$ [Eq. (3)], thus leading to a corresponding density profile $\rho_b(z^\star,t)=\rho_0 - \Delta\rho[C(z^\star,t)-0.5]$. Here, $\Delta\rho$ and ρ_0 denote the difference and the average of the densities of the reacted ($C=1$) and unreacted ($C=0$) fluids. Throughout, we assume that the kinematic viscosity ν and the molecular diffusivity D are constant in the mixture. The analysis is facilitated by considering a moving coordinate system, $z=z^\star - v_r t$. Denote by $\rho=\rho_b+\tilde{\rho}$, $C=C_b+\tilde{C}$, and $P=P_b+\tilde{P}$ the density, concentration, and pressure in the perturbed state. The hydrodynamics are described by the Navier-Stokes equations, under the Boussinesq approximation, averaged across the gap. Under the assumption of a parabolic velocity profile in the gap (valid for large aspect ratio HS cells [11]) and negligible nonlinear terms, this leads to the following 2D incompressible Navier-Stokes-Darcy equation [9,12,21], where the planar velocity $\vec{v}$ in the laboratory frame of reference satisfies:

$$\left(\rho_0\frac{\partial}{\partial t} - \rho_0 v_r\frac{\partial}{\partial z} - \eta\Delta - \frac{\eta}{\kappa}\right)\vec{v} = -\vec{\nabla}P + \rho\vec{g}$$

$$\text{and} \quad \vec{\nabla}\cdot\vec{v} = 0 \tag{5}$$

and where $\kappa = h^2/12$ is the permeability of the cell. The mass conservation of the chemical species under a dilute solution assumption is described by the convection-diffusion-reaction equation

$$\left(\frac{\partial}{\partial t} - v_r\frac{\partial}{\partial z} + \vec{v}\cdot\vec{\nabla}\right)C = D\Delta C + f(C) \tag{6}$$

where C is gap averaged. The NSD equation was shown to describe quite accurately the full 3D problem of the Rayleigh-Taylor instability between miscible fluids in a Hele-Shaw cell [9] (corresponding to $v_r=0$ and $f=0$ in the above two equations).

Consider, next, the linearized forms of Eqs. (5) and (6), using the relation $\tilde{\rho} = -\Delta\rho\tilde{C}$. Then we obtain

$$\rho_0\left(\frac{\partial}{\partial t} - v_r\frac{\partial}{\partial z} - \nu\Delta + \frac{\nu}{\kappa}\right)v_x = -\frac{\partial\tilde{P}}{\partial x}, \tag{7}$$

$$\rho_0\left(\frac{\partial}{\partial t} - v_r\frac{\partial}{\partial z} - \nu\Delta + \frac{\nu}{\kappa}\right)v_z = -\frac{\partial\tilde{P}}{\partial z} - \tilde{\rho}g, \tag{8}$$

$$\frac{\partial v_x}{\partial x} + \frac{\partial v_z}{\partial z} = 0, \tag{9}$$

$$\left(\frac{\partial}{\partial t} - v_r\frac{\partial}{\partial z} - D\Delta\right)\tilde{\rho} = -v_z\frac{\partial\tilde{\rho}}{\partial z} + \tilde{\rho}\left(\frac{df}{dC}\right)_{C_b}. \tag{10}$$

For a cell width sufficiently large compared to a wavelength, the Fourier components of the disturbance with respect to the horizontal coordinate x are independent. Therefore, for a normal mode with wave vector k in the horizontal direction and a corresponding growth rate $\sigma(k)$, the vertical velocity in the perturbed state is $v_z(x,z,t)=w(z)e^{\sigma t+ikx}$, and likewise for the density, pressure, and horizontal velocity. After some calculations, one finds that the vertical disturbance $w(z)$ obeys the following equation:

$$\left(\frac{\sigma}{D} + k^2 - \frac{v_r}{D}\frac{d}{dz} - \frac{d^2}{dz^2} - \frac{1}{D}\frac{df}{dC}\right) \times\left(\frac{\sigma}{\nu} + k^2 - \frac{v_r}{\nu}\frac{d}{dz} - \frac{d^2}{dz^2} + \frac{1}{\kappa}\right)\left(k^2 - \frac{d^2}{dz^2}\right)w = \frac{gk^2}{D\nu\rho_0}\frac{d\rho_b}{dz}w. \tag{11}$$

Given a concentration profile $C(z)$, the dispersion relation $\sigma(k)$ of the above equation can be obtained by various methods, including matched asymptotic expansions for the various wave-number regimes. For convenience, we convert Eq. (11) to dimensionless notation, by choosing the MRT length

$L=(2\rho_0\nu D/\Delta\rho g)^{1/3}$ and the characteristic time $T=L^2/\sqrt{\nu D}$. This selection emphasizes the symmetric role played by viscous and molecular diffusions in the absence of chemical reaction [9]. This leads to the dimensionless wave vector $q=kL$ and dimensionless growth rate $n=\sigma T$, based on which Eq. (11) becomes

$$\left(q_D^2-\frac{(1+2C_S)}{R}\frac{d}{dZ}-\frac{d^2}{dZ^2}\right)\times\left(q_\nu^2-\frac{(1+2C_S)}{RSc}\frac{d}{dZ}-\frac{d^2}{dZ^2}\right)\left(q^2-\frac{d^2}{dZ^2}\right)W=\frac{2q^2}{R}C_b(1-C_b)W. \tag{12}$$

Here, we defined $Z=z/L$, $W=wT/L$, $K=\kappa/L^2$, the Schmidt number $\mathrm{Sc}=\nu/D$, the normalized front width R,

$$R=\frac{l_r}{L}=\sqrt{\frac{2D}{\alpha L^2}}=\frac{D}{Lv_r}(1+2C_S) \tag{13}$$

and the combinations

$$q_D^2=q^2+n\sqrt{\mathrm{Sc}}-\frac{2}{R^2}[C_b(2-3C_b)+C_S(2C_b-1)],$$

$$q_\nu^2=q^2+\frac{n}{\sqrt{\mathrm{Sc}}}+\frac{1}{K}. \tag{14}$$

It is notable that the Hele-Shaw effect enters through the normalized permeability K, which is proportional to the square of the ratio of the two length scales h and L. For a given fluid (D, Sc, and ρ_0) and a given reaction (l_r and $\Delta\rho/\rho_0$) in a Hele-Shaw cell of thickness h, the three lengths that govern the instability are L, h, and l_r (thus defining the parameters K and R).

It is of some interest to delineate the range of physical parameters for which the Darcy, porous media flow regime holds in the range of unstable wavelengths. This is the regime of the long-wave approximation ($q^2K\ll 1$), which requires $K\ll 1$, since q is of order 1. The reported experiments correspond to $K=0.99,1.43,3.21$, values which rule out the use of the Darcy approximation.

IV. SIMULATIONS AND EXPERIMENTAL PARAMETERS

To ascertain the usefulness and relevance of the above 2D averaging, the stability analysis results will be compared to 3D lattice BGK simulations (model $3DQ19$ with 19 directions [9,18,19]), with periodic boundary conditions in the plane of the cell (x direction). The equations simulated are the 3D CDR [Eq. (6)] in a velocity field given by the Navier-Stokes equations. A body force proportional to C is applied to model the gravity force under the Boussinesq approximation. Using as initial condition a base state where C varies according to Eq. (3), we follow the time evolution of a sine perturbation of wavelength λ. In the simulations, the MRT length L is chosen such that, for a given gap cell, the normalized permeability is that of the experiment. 2-D lattice BGK simulations (model $2DQ9$ with nine directions) of the NSD and CDR equations were also performed, and led to results analogous to the 3D simulations. For the sake of comparison, 2D and 3D simulations of the growth of fronts perturbed by random noise are analyzed as in the experiments.

To compare our results with the experimental data [5], we need the three characteristic lengths of the problem. In the IAA reaction experiments, the iodate has an initial concentration $C_0=[\mathrm{IO}_3^-]$ with the initial concentration of the reaction product (iodide I^-) being zero. The value of the positive constant is $C_S=0.0027$. As the reaction proceeds, $[\mathrm{I}^-]$ increases from 0 to C_0 in an autocatalytic way. Thus, in our notation, $C=[\mathrm{I}^-]/C_0$ varies from 0 to 1. Since the reaction occurs in a dilute aqueous solution, the viscosity, molecular diffusion and densities are close to those of pure water: $\nu=(0.99\pm0.05)\times10^{-6}$ m^2/s, $D=2.04\times10^{-9}$ m^2/s, and $\rho_0=1001.98\pm0.01$ kg/m^3. Also, as the thermal diffusivity is larger than the mass diffusivity, the effect of temperature on density can be neglected [13]. Using as density difference the value $\Delta\rho=(135\pm15)\times10^{-6}$ kg/m^3, we get the MRT characteristic length $L=145\pm5$ μm. The three cell thicknesses investigated were $h=500$, 600, and 900 μm, corresponding to dimensionless permeabilities $K=0.99$, 1.43, and 3.21, respectively. The reaction rate α must be deduced from the velocity measured on traveling fronts, $v_r=23.6\pm0.1$ μm/s, from which we can get the reaction width $l_r=D(1+2C_S)/v_r=86$ μm, further yielding $R=l_r/L=0.60$ and $\alpha=2D/l_r^2=0.55$ s^{-1}.

V. RESULTS AND DISCUSSION

As a benchmark test, the different 2D linear analyses were compared to 3D simulations, carried out with the parameter values given above, and with a thickness corresponding to the normalized permeability $K=3.21$. In the simulations, each growth rate is measured during the early exponential development of a one-mode sine perturbation. Therefore, the 3D simulations reproduce the exact physical situation addressed by the 2D linear analyses. The growth rates so obtained are displayed in Fig. 1 (circles), together with the normalized dispersion curves, $n=\sigma T$ vs $q=kL$, corresponding to the various models, namely, the Darcy-CDR (dot-dashed line), the NSD-eikonal (dashed line), and the NSD-CDR (solid line) models. Both the Darcy-CDR and the NSD-eikonal models overpredict the values for the maximum growth rate, the corresponding wave vector, and the cutoff wave vector. In particular, Fig. 1 clearly shows that the Darcy description is not valid in this range of normalized permeabilities (where $K>1$). On the other hand, the NSD-CDR dispersion curve falls very closely on the 3D simulation points, demonstrating that the overall physics are correctly captured by the gap-averaged 2D model.

Figure 2 shows that the NSD-CDR curve also compares better with the experimental measurements (crosses) than the NSD-eikonal model. However, it still overestimates the ex-

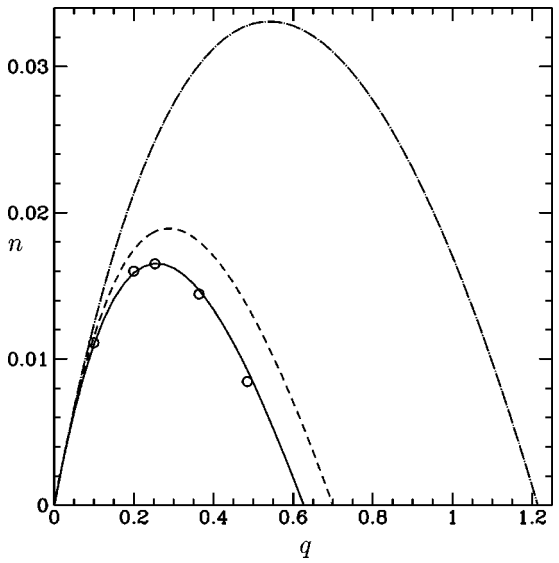

FIG. 1. Normalized dispersion relations, $n=\sigma T$ vs $q=kL$, for the Rayleigh-Taylor instability of an autocatalytic front with the same parameters as in [5]: the miscible Rayleigh-Taylor length $L=(2\rho_0\nu D/\Delta\rho g)^{1/3}=145$ μm, the characteristic time $T=L^2/\sqrt{\nu D}$, and the dimensionless permeability $K=h^2/12L^2=3.21$, corresponding to a cell thickness $h=900$ μm. The curves show the numerical solutions of the eigenvalue problem, using Darcy's law with the convection-diffusion-reaction equation (dot-dashed line), the Navier-Stokes-Darcy approximation with the eikonal equation (dashed line), and the NSD with the CDR equation (solid line). The circles are the results of 3D lattice BGK simulations of the growth of sine perturbations.

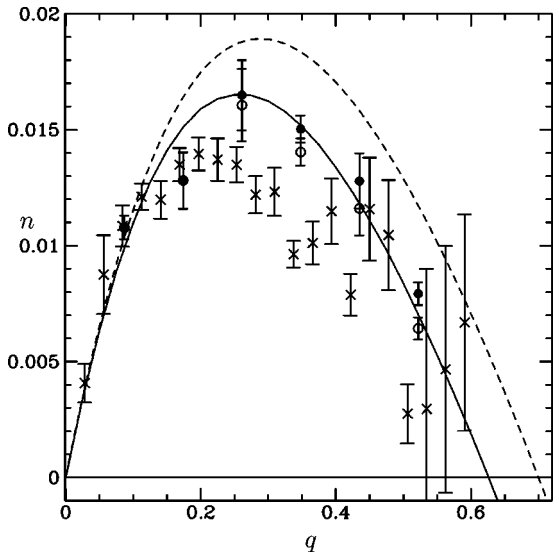

FIG. 2. Comparison of the normalized dispersion relations, n vs q (lines), with the experimental data (crosses) obtained in a cell of thickness $h=900$ μm and of dimensionless permeability $K=3.21$. Dashed and solid lines correspond to the NSD-eikonal equations and the NSD-CDR equations, respectively. Open and full circles are the results of 3D and 2D lattice BGK simulations, respectively, of the growth of perturbed fronts.

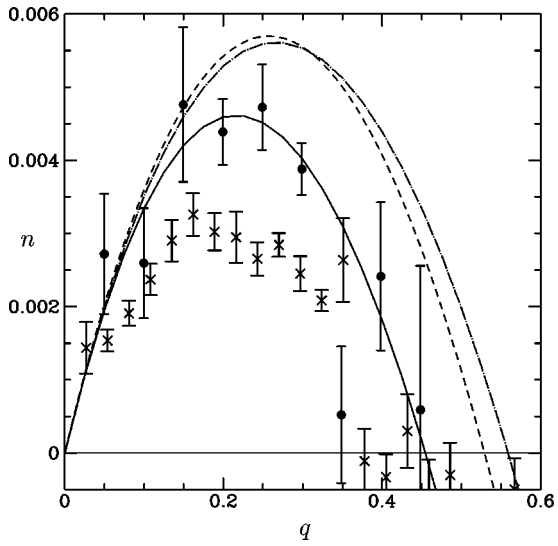

FIG. 3. Comparison of the normalized dispersion relations, n vs q (lines), with the experimental data (crosses) obtained in a cell of thickness $h=500$ μm and of dimensionless permeability $K=0.99$. The lines correspond to Darcy's law with CDR equation (dot-dashed), the NSD-eikonal equations (dashed), and the NSD-CDR equations (solid). The circles are the results of 2D simulations of the growth of perturbed fronts.

perimental values of the maximum. As this slight discrepancy could be due to the interplay between different modes in the experiment, 3D simulations of the evolution of interfaces perturbed by random noise and 2D simulations based on the NSD equation with identical initial conditions were performed. To determine the growth rates, the fronts so obtained were subject to the same data processing as in the experiments. The 3D (open circles) and 2D (full circles) results are displayed in Fig. 2. The two sets of data compare fairly well with each other and with the NSD-CDR curve, thus confirming the ability of the NSD equation to accurately model in two dimensions the 3D instability phenomenon, and suggesting that the model still applies when different modes act together at the interface.

Figure 3 displays the result obtained for the smallest cell gap, $K=0.99$. The 2D simulation points (full circles) again fall on the NSD-CDR model dispersion curve. Surprisingly enough, the Darcy-CDR and NSD-eikonal models predict almost the same dispersion curves which, however, are above both experimental and simulation points, indicating that Darcy's equation should not be used for this normalized permeability, which is still not small enough. We note that, for this cell thickness, the NSD-CDR predictions are slightly above the experimental points. The same trend can be noticed in Fig. 4, which displays the dispersion curves obtained for the case $K=1.43$. Although the NSD-CDR model is closest to the experimental values, it still overestimates the maximum growth rates.

We remark that, if this discrepancy were to be relevant, it could be attributed to nonlinearity effects, for example, caused by the finite amplitude of the experimental unstable modes. It is also worth noticing that in both the model and the simulations the interface is assumed to be symmetric with respect to the midplane of the cell. Lack of validity of

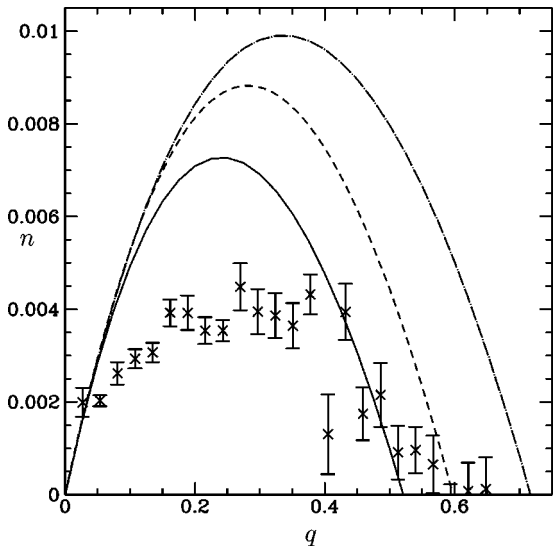

FIG. 4. Comparison of the normalized dispersion relations, n vs. q (lines), with the experimental data (crosses) obtained in the cell of thickness $h=600$ μm and of dimensionless permeability, $K=1.43$. The lines correspond to Darcy's law with CDR equations (dot-dashed), the NSD-eikonal equations (dashed), and the NSD-CDR equations (solid).

this hypothesis could also provide an explanation for the overestimation of the observed maximum growth rate. On the other hand, the discrepancy at the maximum may not be significant, as the bars on the experimental points represent the rms of the measurements performed on several experiments, rather than the actual error bars, the estimation of which is nearly impossible for this type of data processing. Moreover, the noisy nature of the experimental dispersion curves (especially in Fig. 4, $K=1.43$) indicates that they should not be fully trusted, without question.

VI. CONCLUSIONS

We have extended our previous work on the linear stability analysis of miscible fluids in a Hele-Shaw cell [9], by adding a chemical reaction term to the convection-diffusion equation. The stability of the resulting chemical front, propagating in a vertical Hele-Shaw cell, was analyzed. We used the Navier-Stokes-Darcy equation to describe the gap-averaged 2D flow and the full convection-diffusion-reaction equation to describe the evolution of the concentration. Applied to the case of the IAA reaction, this analysis is found to give a better fit of both the experimental data [5] and the data obtained by lattice BGK numerical simulations, compared to previous analyses, such as NSD-eikonal and Darcy-CDR models. Moreover, within the framework of the present analysis, different regimes of instability can be identified, depending on the relative values of the three lengths of the problem, namely, the MRT length $L=(2\rho_0\nu D/\Delta\rho g)^{1/3}$, the chemical front width l_r, and the cell thickness h. As the reported experiments correspond to the dimensionless permeabilities, $K=h^2/12L^2=0.99,1.43,3.21$, and $R=l_r/L=0.60$, the Darcy-CDR model, valid for $K\ll 1$, does not hold. This was convincingly demonstrated in the case of the thicker cell. The deviation of the experimental data from the NSD-CDR dispersion curves is about two times smaller than that with the NSD-eikonal model. However, the predictions of the latter model are surprisingly good for a model that does not account for the reaction rate and the front width and velocity. But there is little chance for these fortuitous predictions to hold for other chemical reaction parameters. On the contrary, the NSD-CDR model should be robust concerning changes of parameters either in geometry (h), chemistry (l_r), or fluid (L). Moreover, the 2D model could be useful in addressing the nonlinear development regime of unstable fingers.

ACKNOWLEDGMENTS

This work was part of IDRIS Project No. 014052, and was partially supported by CNES through Grant No. 793/CNES/00/8368, and ESA through Grant No. AO-99-083.

[1] S. K. Scott, *Oscillations, Waves and Chaos in Chemical Kinetics* (Oxford University Press, Oxford, 1994).
[2] A. Hanna, A. Saul, and K. Showalter, J. Am. Chem. Soc. **104**, 3838 (1982).
[3] J.A. Pojman, I.R. Epstein, T.J. McManus, and K. Showalter, J. Phys. Chem. **95**, 1299 (1991).
[4] M.R. Carrey, S.W. Morris, and P. Kolodner, Phys. Rev. E **53**, 6012 (1996).
[5] M. Böckmann and S.C. Müller, Phys. Rev. Lett. **85**, 2506 (2000).
[6] Lord Rayleigh, *Scientific Papers* (Cambridge University Press, Cambridge, England, 1900), Vol. 2, pp. 200–207.
[7] G.I. Taylor, Proc. R. Soc. London, Ser. A **201**, 192 (1950).
[8] S. Chandrasekhar, *Hydrodynamic and Hydromagnetic Stability* (Oxford University Press, 1961), and references therein.
[9] J. Martin, N. Rakotomalala, and D. Salin, Phys. Fluids **14**, 902 (2002).
[10] J. Fernandez, P. Kurowski, P. Petitjeans, and E. Meiburg, J. Fluid Mech. **451**, 239 (2002).
[11] J. Huang, D.A. Vasquez, B.F. Edwards, and P. Kolodner, Phys. Rev. E **48**, 4378 (1993).
[12] J. Huang and B.F. Edwards, Phys. Rev. E **54**, 2620 (1996).
[13] J.W. Wilder, B.F. Edwards, and D.A. Vasquez, Phys. Rev. A **45**, 2320 (1992).
[14] D.A. Vasquez, J.M. Littley, J.W. Wilder, and B.F. Edwards, Phys. Rev. E **50**, 280 (1994).
[15] D.A. Vasquez and C. Lengacher, Phys. Rev. E **58**, 6865 (1998).
[16] D.A. Vasquez, J.W. Wilder, and B.F. Edwards, J. Chem. Phys. **104**, 9926 (1996).

[17] A. De Wit, Phys. Rev. Lett. **87**, 054502 (2001).
[18] N. Rakotomalala, D. Salin, and P. Watzky, J. Fluid Mech. **338**, 277 (1997).
[19] P. Gondret, N. Rakotomalala, M. Rabaud, D. Salin, and P. Watzky, Phys. Fluids **9**, 1841 (1997).
[20] J.H. Merkin and H. Ševčíková, Phys. Chem. Chem. Phys. **1**, 91 (1999).
[21] P. Gondret and M. Rabaud, Phys. Fluids **9**, 3267 (1997).